Microcavity exciton-polariton mediated Raman scattering: Experiments and theory

A. Bruchhausen,[*] L. M. León Hilario, A. A. Aligia,[†] A. M. Lobos,[‡] and A. Fainstein[†]

Instituto Balseiro & Centro Atómico Bariloche, CNEA, R8402AGP Bariloche, Rio Negro, Argentina

B. Jusserand

Institut des NanoSciences de Paris, UMR CNRS 7588, Université Pierre et Marie Curie, Campus Boucicaut, 140 Rue de Lourmel, 75015 Paris, France

R. André

Laboratoire de Spectrométrie Physique, Université Joseph Fourier-Grenoble 1, CNRS, Boîte Postale 87, F-38402 St. Martin d'Heres Cedex, France

(Received 16 May 2008; published 29 September 2008)

We studied the intensity of resonant Raman scattering due to optical phonons in a planar II-VI-type semiconductor microcavity in the regime of strong coupling between light and matter. Two different sets of independent experiments were performed at near outgoing resonance with the middle polariton (MP) branch of the cavity. In the first, the Stokes-shifted photons were kept at exact resonance with the MP, varying the photonic or excitonic character of the polariton. In the second, only the incoming light wavelength was varied, and the resonant profile of the inelastic scattered intensity was studied when the system was tuned out of the resonant condition. Taking some matrix elements as free parameters, both independent experiments are quantitatively described by a model which incorporates lifetime effects in both excitons and photons, and the coupling of the cavity photons to the electron-hole continuum. The model is solved using a Green's function approach which treats the exciton-photon coupling nonperturbatively.

I. INTRODUCTION AND MOTIVATION

Semiconductor microcavities (MC's) are micron-scaled photonic structures, consisting of two planar distributed Bragg reflectors (DBR's) separated by a spacer with a thickness of the order of the photon wavelength, forming a high quality Fabry-Pérot resonator, and leading to a localized photonic mode inside the MC.[1] This spacer usually embeds quantum wells (QW's) conveniently located at the antinodes of the optical-cavities electric field. The strong vertical confinements of both the electric field and the QW excitons result in a strong and by design controllable light-matter interaction. When this MC mode is resonant with the excitonic transitions, and when the lifetime broadening of the MC photons (γ_f) and QW excitons (γ_e) is smaller than the photon-exciton interaction (Ω), the system is under the strong-coupling regime, where coherent Rabi oscillations between the bare states occur. This regime is evidenced by the characteristic anticrossing behavior exhibited by the exciton and the cavity mode when they are brought into resonance. As a consequence, the "new" eigenstates of the system are strongly mixed exciton-photon states, *cavity polaritons*.[1–4] These quasiparticles have been shown to exhibit a large number of interesting properties, most of them arising from their inherited bosonic character. This character together with their very small effective mass (typically 10^{-4} times smaller than that of the bare excitons) enables processes like the condensation into a quantum degenerate Bose-Einstein state[5,6] in thermal equilibrium with the lattice,[7] and the *boser* effect or stimulated emission,[8–10] among other nonlinear phenomena.[11] This made the cavity-polariton systems not only very interesting from the basic fundamental point of view, but also very promising in the field of technological application in coherent light emitting devices.[2–4,11,12] Efforts have been devoted incessantly to the study of cavity polaritons experimentally and theoretically during the last 15 years,[2–4] since the first experimental observation.[13]

The process of inelastic light scattering due to vibrations in semiconductors and in microcavities for the case where the energy of the light mode is far from the corresponding one of electronic excitations is usually very well described by treating the light-matter coupling perturbatively.[14,15] In this case the Raman effect is mediated by electronic or excitonic states by a second-order process in exciton-photon interaction. Instead, in microcavities when the cavity mode is tuned near the QW-exciton energy the perturbative approach fails.[16–20] The exact treatment of the light-matter interaction, i.e., the cavity exciton-polariton picture, is essential and the inelastic process (now mediated by polaritons) must be described by a first-order perturbation theory of the polariton-phonon interaction.[16,18,21]

Since the Raman process due to optical phonons is a coherent process, it is very sensitive to the damping of the resonant state.[16–19] Resonant Raman scattering (RRS) experiments as a function of photon-exciton detuning evidence the dependence of the polariton-phonon and polariton-external-photon coupling with the mode mixing in the process. This is distinctly demonstrated by the maximum in the scattering efficiency near the mode anticrossing (zero detuning) and the decreasing efficiency when the polariton character approaches either the pure exciton or pure photon state.[18,19] Although existing simplified theoretical models describe the phenomenological and qualitative behavior of the experimental results, the relevance of rigorously including polariton dephasing and dumping effect has been strongly emphasized.[17,19,22]

In this paper we present detailed RRS experimental results together with a theoretical improvement of the existing models that rigorously takes polariton lifetimes into account. The experiments are performed on II-VI semiconductor based microcavities and consist essentially of two types: the first showing the behavior of the Raman intensity as a function of cavity-photon-exciton detuning at exact resonance, and the second showing the behavior of the outgoing scattered process for a fixed detuning, and performing a scan with the excitation energy. Experiments are compared to the developed theory that uses a Green's function approach to include the damping effects and the electron-hole (free-exciton) states in a formal way. Using the matrix elements in the theory as free parameters, the theory describes accurately the Raman intensity simultaneously for both types of experiments. Bare lifetime broadening is obtained from a fitting procedure and the effects of the exciton lifetime in relation to the cavity-polariton lifetime are discussed. An important improvement to the previously presented theoretical approaches[23,24] to describe the experimental observations quantitatively is obtained in the present work by accounting also for the second type of experiment, which provides additional severe constraints to the unknown parameters of the theory.

The paper is organized as follows: In Sec. II the samples are shortly described and the experiments are presented. In Sec. III the experimental results are shown. The theoretical model is introduced in Sec. IV: A short description of the existing phenomenological approaches is given, and afterwards the model Hamiltonian and Green's function approach for the Raman intensity are explained. In Sec. V the experimental and calculated results are analyzed and discussed. Finally the conclusions of this work are summarized.

II. EXPERIMENTAL DETAILS

Experiments are all performed on a II-VI semiconductor microcavity. CdTe-based cavities are interesting since excitonic binding energies in CdTe quantum wells are much larger (~ 25 meV) as compared to GaAs (~ 10 meV). This is a consequence of a stronger electron-hole attraction that makes the excitonic states in these compounds much more stable. In addition, the ionic character of these compounds leads to a stronger light-matter coupling and hence to much larger Rabi gaps and stronger polaritonic effects compared to the GaAs-based structures. On the other hand Raman efficiency due to optical phonons is also larger allowing clearer studies, especially when the Stokes-shifted photon is tuned at near resonance to a polaritonic state, where luminescence hinders its observation.

The studied cavity was grown (100)-oriented by molecular beam epitaxy, and consists of two distributed Bragg reflectors (DBRs) enclosing a $\lambda/2$ $Cd_{0.4}Mg_{0.6}Te$ spacer. Three centered CdTe quantum wells of nominal width 72 Å and separated by 69 Å from each other are embedded in the spacer. The cavity mirrors consisted of 15.5 periods of $Cd_{0.4}Mg_{0.6}Te/Cd_{0.75}Mg_{0.25}Te$ $\lambda/4$ layers for the top DBR, and 21 pairs for the DBR at the bottom, to balance the effect of the air-substrate asymmetry. The layers were grown in
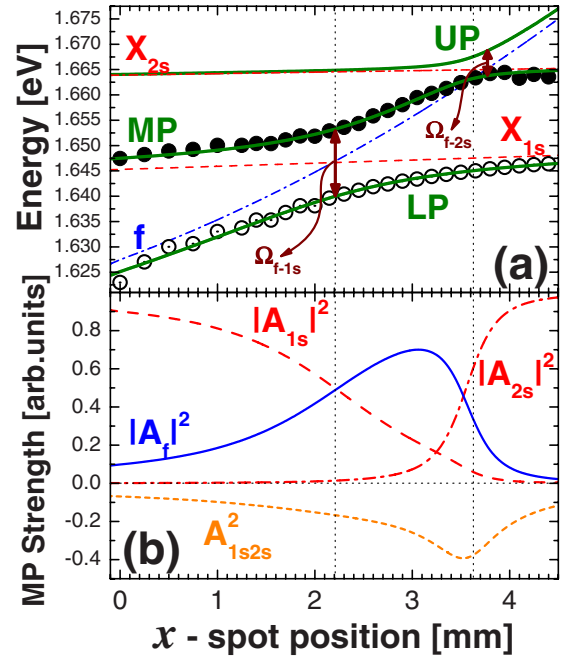

FIG. 1. (Color online) (a) Dispersions of the cavity-polariton modes as a function of the spot position on the sample, derived from photoluminescence. Experimental data: LP (empty dots) and MP (solid dots) branches. The full lines are a fit to the experiments with a three-coupled-mode model, using the plotted bare cavity-photon (f, dashed-dotted) and exciton (X_{1s} and X_{2s}, dashed) curves, and Rabi splitting of $\Omega_{f-1s} \simeq 13$ meV and $\Omega_{f-1s} \simeq 3.5$ meV, as input. (b) Photon ($|A_f|^2$, full line) and exciton ($|A_{1s}|^2$ and $|A_{2s}|^2$, dashed and dashed-dotted lines) strengths of the MP, derived from the fit in panel (a). $A_{1s2s}^2 = A_{1s}A_{2s}^* + A_{1s}^*A_{2s}$ (short dashes) is the exciton crossed interference term.

such a way that their thickness decreases in one direction (like in a wedge), and the cavity mode can thus be tuned by displacing the position of the laser spot on the sample. Experiments were performed at back-scattering $z(x,x')z'$ geometry, where $z(z')$ and $x(x')$ describe the incident (scattered) beam direction and light polarization, respectively.[25] Here, x and x' correspond to the (110) direction, z to the (001) epitaxial growth direction, and since the configuration is back-scattering, $z' \equiv \bar{z}$. A tunable cw Ti:sapphire laser was used as excitation source at near normal incidence, with power $\lesssim 50$ μW, and focalized to a spot of $\varnothing \sim 50$ μm. The fixed collection cone normal to the sample surface was $\sim 3°$, corresponding to an uncertainty in the in-plane wave vector of $k_{\parallel} \approx 4.2 \times 10^3$ cm^{-1}. A liquid-He cryostat was used to set the temperature at 4.5 K. At this temperature, the sample shows a double anticrossing of the cavity mode with both the $E1H1(1s)$ (X_{1s}) and the $E1H1(2s)$ (X_{2s}) heavy-hole exciton modes. The dispersion of the middle and lower polariton branches (MP and LP, respectively) derived from photoluminescence experiments is displayed in Fig. 1(a) as function of the spot position x (in mm) on the sample. Unfortunately no direct observation of the presence of the upper polariton (UP) branch was found with luminescence. Using a simple three-coupled-mode model, the best fits of the experimental MP and LP branches were obtained for a Rabi splitting of $\Omega_{f-1s} \simeq 13$ meV and $\Omega_{f-2s} \simeq 3.5$ meV between the cavity

mode and the $1s$ and $2s$ excitons, respectively. The dashed and dashed-dotted lines correspond to the bare (noninteracting) exciton (X_{1s} and X_{2s}) and cavity-photon (f) dispersions used in the model, respectively.[19] The vertical dotted lines indicate the positions of the anticrossings, i.e., the minimal distance between the MP-LP branches and the UP-MP branches. The slight positive slope of the bare exciton dispersions is due to the small thickness gradient, which also affects the QW's.

Two different and independent Raman experiments were performed observing the inelastic scattered photons due to the Raman allowed CdTe QW longitudinal optical (LO) phonons. These phonons have an energy of ~ 172 cm^{-1} (~ 21.3 meV). The first experiment consisted in setting the Stokes-shifted photons always at exact outgoing resonance with the MP, and changing the cavity-photon-exciton detuning by displacing the laser spot on the sample, as described in Refs. 18 and 19. The second experiment consisted in keeping the detuning fixed (i.e., at a fixed spot position), and varying the laser energy at near outgoing resonance, in order to scan the MP with the Stokes-shifted photons. In both cases the spectra were analyzed using a Jobin-Yvon T64000 triple spectrometer in subtractive mode, equipped with a liquid-N$_2$-cooled charged-coupled device (CCD).

III. EXPERIMENTAL RESULTS

Typical spectra for the RRS experiment (of the first kind described in Sec. II) are shown in Fig. 2(a), for different MP mode energies (i.e., laser spot positions). The Raman peak is highlighted on top of the MP luminescence. For each spectrum the exact resonance was set tuning the laser energy in order to maximize the Raman peak intensity.

In the bottom panel [Fig. 2(c)] the Raman intensity, derived from the spectra in panel (a), is shown as function of the MP energy. As additional information in the center panel [Fig. 2(b)] the difference between the measured MP and LP energies is also displayed. The full (dashed) line corresponds to the calculated differences $E_{MP}-E_{LP}$ ($E_{UP}-E_{MP}$), using the fitted curves and parameters of Fig. 1(a) obtained from the three-coupled-mode model. The vertical dotted lines indicate the anticrossing positions, i.e., the minima of the respective energy differences.

In Fig. 2(a), for low MP energies, luminescence corresponding to localized excitonic states (labeled as X_{loc}) can be distinguished.[18] Moreover, for increasing MP energies, i.e., for increasing photon-X_{1s} detuning, the overwhelming LP luminescence appears from the left. One thing to notice is how the MP luminescence increases when its energy approaches the X_{2s} exciton at ~ 1.665 eV. Note that the luminescence maximum is reached slightly below this energy. This typical behavior of luminescence in the presence of an anticrossing is referred to as "cavity pulling," in this case between the MP and the UP.[26] A similar behavior is observed for the luminescence coming from the LP branch, slightly before the anticrossing of the MC photon and the X_{1s} exciton.

As for the second type of experiment, typical first-order LO-phonon Raman scans for varying laser energy close to outgoing resonance with the MP at two different spot posi-
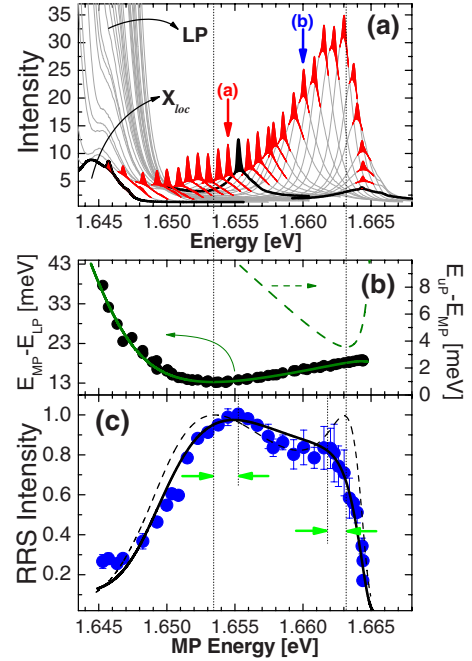

FIG. 2. (Color online) (a) Raman spectra at exact outgoing resonance with the MP for varying detuning. The Raman peaks are indicated by the filled areas on top of the MP luminescence. The arrows labeled as (a) and (b) indicate the equivalent positions of the Raman scans of Figs. 3(a) and 3(b), respectively. (b) Experimental and fitted differences between the energies of the MP and LP branches (left axis), and UP and MP (right axis), as function of the MP energy derived from Fig. 1(a). (c) Resonant Raman intensity (full dots) derived from panel (a). The dashed curve corresponds to the calculation using the simple model without damping effects, and the full curve corresponds to the fit using the theory derived in the text. The vertical dotted lines indicate the position of both anticrossings. The horizontal arrows in panel (c) indicate the shift of the RRS intensity maxima. Since the Stokes-shifted photon is at exact resonance, its energy coincides with the MP energy for each particular detuning.

tions (i.e., detunings) are shown in Fig. 3. In Fig. 3(a) the MP is centered at ~ 1.6548 eV (corresponding to a spot position on the sample of about $x \simeq 2.5$ mm), whereas in Fig. 3(b) it is centered at ~ 1.6599 eV (for $x \simeq 3.1$ mm). The spectra corresponding to the outgoing MP resonant condition are displayed with thicker lines, and the corresponding equivalent resonant spectra are indicated with arrows in Fig. 2(a). Note that the photoluminescence background of both scans in Fig. 3 differs considerably, as is clearly observed in the corresponding resonant spectra on Fig. 2(a). Figure 4 shows the Raman intensity profiles (a) and (b) derived, respectively, from Figs. 3(a) and 3(b). A third profile (c) is also displayed, which corresponds to an energy of the MP at ~ 1.6533 eV (for a spot position $x \simeq 2.2$ mm).[27] Note the asymmetry of the intensity scans labeled as (a) and (c) in Fig. 4 toward lower energies. This might be ascribed to the strong presence of the LP. At lower energies, the tail of the strong resonance of the LP mode, which is overwhelmingly larger, starts to contribute to the Raman peak intensity, thus inducing the asymmetry in the Raman scan. Scans (a) and (c) are taken near the anticrossing, where both branches (MP and

FIG. 4. (Color online) Raman intensity scans as a function of the Stokes-shifted energy for varying laser energy close to the MP outgoing resonance for three different detunings. The MP energy corresponds, respectively, to (a) $E_{MP} \sim 1.6548$ eV, (b) ~ 1.6599 eV, and (c) ~ 1.6533 eV. The positions on the sample are (a) $x \simeq 2.5$ mm, (b) $\simeq 3.1$ mm, and (c) $\simeq 2.2$ mm. The Raman intensity resonates at the MP energy. The experimental intensities labeled as (a) and (b) are derived from the spectra shown in Figs. 3(a) and 3(b), respectively. The full lines are a fit to the data using the theory derived in the text (Sec. IV).

$$H_f = E_f f^\dagger f + \sum_p \epsilon_p r_p^\dagger r_p + \sum_p (V_p r_p^\dagger f + \text{H.c.}). \quad (2)$$

Here $f^\dagger$ creates a MC photon, which is hybridized to a continuum of radiative modes described by creation operators $r_p^\dagger$. The effect of the latter is to provide a finite lifetime (γ_f) to the cavity mode, even in the absence of light-matter interactions.

Similarly, the excitonic part of H is described as

$$H_e = \sum_i E_i e_i^\dagger e_i + \sum_{iq} \epsilon_{iq} d_{iq}^\dagger d_{iq} + \sum_{iq} (V_{iq} d_{iq}^\dagger e_i + \text{H.c.}), \quad (3)$$

where $e_i^\dagger$ creates exciton states that will couple strongly to the cavity-photon mode. For example $e_1^\dagger$ creates a $1s$ exciton state of energy E_{1s}. Analogous to the case of the MC photon, we assume that each exciton mode mixes with a continuum of bosonic excitations (described by the operators $d_{ig}^\dagger$), which broadens its spectral density. The effect of this mixing is to introduce a broadening γ_{ei} for the excitons even without interaction with the light. The detailed description of this broadening is beyond the scope of this work. Numerous physical mechanisms are known to contribute to the damping of the excitonic wave function and hereby to the line broadening. Some of them are, for example, impurities, defect-scattering, interface roughness, well-width fluctuations, and alloy disorder, which have been demonstrated to be present in this kind of II-VI based microcavities.[30] Whittaker[31,32] has shown that the inhomogeneous broadening introduced by disorder can be described accurately introducing an imaginary part in the self-energy of the exciton Green's function. As we will show below, H_e has a similar effect within our theory. Therefore the broadenings γ_{ei} [see Eq. (18)] can be regarded as due to lifetime broadening.

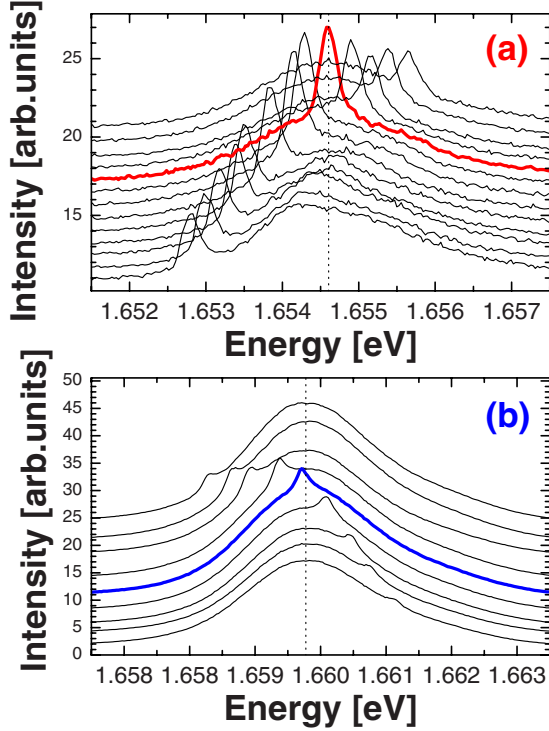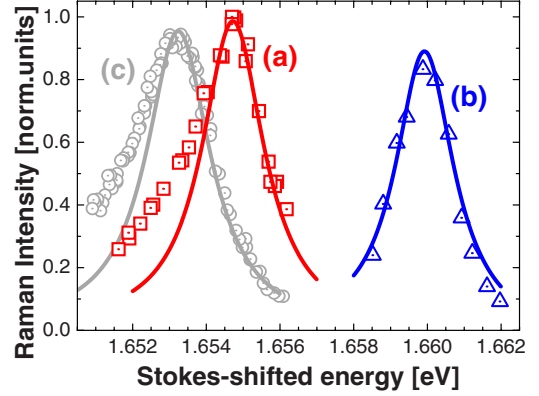The third term in Eq. (1) describes the electronic excita-

---

FIG. 3. (Color online) Outgoing Raman scans for a fixed photon-exciton detuning, and varying laser excitation energy. Scan (a) corresponds to a spot position of $x \simeq 2.5$ mm and (b) to $x \simeq 3.1$ mm. The Raman peak moves on top of the broad MP luminescence peak and resonates at its position, indicated by the vertical dotted line. The resonant situation is highlighted with a thicker curve, and corresponds to the positions indicated with vertical arrows in Fig. 2, and labeled with (a) and (b), respectively. Note that the broad luminescence peak in (b) is ~ 3 times larger than in (a).

LP) are closer to each other. This is not the case for scan (b) [see Figs. 3(b) and 4]. This scan is far from the LP and at this detuning its resonant contribution is less strong. Thus this intensity scan is more symmetric.

In Sec. IV the theoretical background will be addressed, the Green's function formalism presented, and the calculation of the Raman intensity within this model will be described.

IV. THEORETICAL DESCRIPTION

A. Model

In a cavity-polariton system, only MC confined photons and QW confined excitons with the same in-plane wave vector ($k_\parallel$) are coupled.[28] Since the above described experiments are performed in near-backscattering geometry, i.e., $z(x',x')\bar{z}$, $k_\parallel$ is considered to be zero ($k_\parallel = 0$).[29] In what follows the total wave vector and polarization indices will be suppressed, in order to simplify the notation.

The following Hamiltonian, for a given $k_\parallel$, is considered to describe the cavity exciton-polariton system:[23]

$$H = H_f + H_e + H_c + H_{\text{mix}}. \quad (1)$$

The first term corresponds to the photonic part of the Hamiltonian:

tions that do *not* couple strongly to the MC photon mode,

$$H_c = \sum_k \epsilon_k a_k^\dagger a_k. \tag{4}$$

These states include discrete exciton states as well as states of the exciton continuum (i.e., the continuum of electron-hole excitations). The latter correspond to the eigenstates of the exciton hydrogen-like Hamiltonian that are not bound and have positive internal energy.[33,34] The operators, which describe this exciton continuum, can be well approximated by $a_k^\dagger = c_k^\dagger v_k$, where v_k destroys a valence electron with two-dimensional (2D) wave vector k and polarization σ, and $c_k^\dagger$ creates an electron in the conduction band with the same k and σ (so that the total wave vector $k_\parallel = 0$). Note that the commutator $[a_k, a_k^\dagger] = v_k^\dagger v_k - c_k^\dagger c_k$. For the temperatures and laser intensities of the experiments, all valence (conduction) states are practically occupied (unoccupied) and therefore with high accuracy $v_k^\dagger v_k = 1$ ($c_k^\dagger c_k = 0$). Therefore the operators entering Eq. (4) can be regarded as ordinary bosons.[35,36]

The separation of the bound excitonic states into those included in H_e or H_c is in principle arbitrary. In particular, when the width of the weakly bound excitonic states near the bottom of the gap is larger than the separation in energy between two next states, these states can be well described as a continuum, beginning at some energy E'_{X_c}, slightly below the energy of the first excitonic state not included in H_e. In our specific treatment for the experimentally studied sample, we describe all states included in H_c as a continuum beginning at E'_{X_c}, and include the two lowest excitonic states (E_{1s} and E_{2s}) that couple "strongly" to the MC photon in H_e. For simplicity we take $E'_{X_c} = E_{2s}$.

Finally, the last term of the Hamiltonian [Eq. (1)] describes the mixing between light and matter:

$$H_{\text{mix}} = \sum_i (V_i e_i^\dagger f + \text{H.c.}) + \sum_k (V_k a_k^\dagger f + \text{H.c.}). \tag{5}$$

According to the quantum theory of radiation, in the dipolar approximation V_k is proportional to $\langle k_c | p_\sigma | k_v \rangle$, where p_σ is the momentum operator in the direction of the electric field, and $|k_c\rangle$ ($|k_v\rangle$) is the wave function which corresponds to the operator c_k (v_k). For simplicity, we are neglecting terms which do not conserve the number of bosons. They can be included without much complication, but their effect is small for the energies of interest.[37]

The Hamiltonian [Eq. (1)] is quadratic and can be formally diagonalized by a Hopfield transformation to the form

$$H = \sum_\nu E_\nu p_\nu^\dagger p_\nu, \tag{6}$$

where the generalized polariton operators $p_\nu^\dagger$ are related to the creation operators entering Eq. (1) by the linear combination

$$p_\nu^\dagger = \sum_j A_{\nu j} \beta_j^\dagger. \tag{7}$$

$\beta_j^\dagger$ stands for any operator entering Eq. (1), and $A_{\nu j}$ are the coefficients that give the (detuning dependent) corresponding photonic or excitonic weight of the polariton state ν.

Note that if only the first terms in Eqs. (2), (3), and (5) are kept, the simple standard coupled-mode model is obtained.[19,22] For instance, the three-coupled-mode model results, when the MC mode couples strongly only to the $i = 1s$ and the $i = 2s$ exciton states, and the values of the interaction are given by $2V_1 \equiv \Omega_{f-1s}$ and $2V_2 \equiv \Omega_{f-2s}$, as it is the case for the above described experiments.

B. Raman intensity

It has been shown previously[18,19,22–24] that the outgoing Raman cross section mediated by cavity polaritons can be calculated by first-order perturbation theory as

$$I(\omega) \propto T_i W_{i \to s} T_s, \tag{8}$$

where T_i describes the incoming channel, i.e., the conversion of the incident external photon to the initial polariton state inside the sample. For the case of outgoing resonance and the scattering geometry used in the experiments, T_i is essentially proportional to the DBR's residual transmission, and can be taken as constant. $W_{i \to s}$ is the scattering probability from the initial $|i\rangle$ to the final $|s\rangle$ polariton state per unit of time. T_s describes the transmission of the final polariton states to the final photon state outside the sample, which is detected. Since the final polariton state leaves the sample due to its photonic part, T_s is essentially the projection of the polariton state on the final photon continuum state, and is thus proportional to the mediating polaritons photon strength, given by $|A_{\nu f}|^2$.

We will center our attention on $W_{i \to s}$, which actually describes the *inelastic scattering process* itself. The transition probability is given by Fermi's golden rule as

$$W_{i \to s} = \frac{2\pi}{\hbar} |\langle i | H' | s \rangle|^2 \rho(\omega), \tag{9}$$

where the initial polariton state is $|i\rangle = p_{\nu'}^\dagger |0\rangle$, the final state is given by $|s\rangle = p_\nu^\dagger b^\dagger |0\rangle$, where $b^\dagger$ creates a LO phonon, and H' is the interaction between polaritons and LO phonons (e.g., Fröhlich interaction) through the excitonic part of the former. $\rho(\omega)$ stands for the density of final polariton states and is given by

$$\rho(\omega) = \sum_\nu \delta(\omega - E_\nu). \tag{10}$$

Since the Hilbert space defined by Eqs. (6) and (7) is infinite, it is cumbersome to work with the eigenstates and eigenenergies. However, we do not need them to obtain the intensity of the Raman scattering process. It is enough to use retarded Green's functions that involve the photon and exciton operators ($\beta_j^\dagger$). These functions $G_{jl}(\omega) = \langle\langle \beta_j ; \beta_l^\dagger \rangle\rangle_\omega$ can be obtained solving a system of equations derived from the equations of motion for the Green's function:

$$\omega \langle\langle \beta_j ; \beta_l^\dagger \rangle\rangle_\omega = \delta_{jl} + \langle\langle [\beta_j, H]; \beta_l^\dagger \rangle\rangle_\omega. \tag{11}$$

The polariton-phonon interaction H' is proportional to the exciton part of the scattered polariton. Thus, for the case of a system where only two exciton states interact strongly with the MC mode, the Raman intensity of Eq. (8) results proportional to

$$I(\omega) \propto |A_{\nu f}|^2 |A_{\nu e1} + \alpha A_{\nu e2}|^2 \rho(\omega), \quad (12)$$

where ν is the label of the polariton eigenstate such as $E_\nu = \omega$.

Here we are neglecting the contribution of the electron-hole continuum to H', and α represents the ratio of matrix elements of the exciton-LO phonon interaction between $2s$ and $1s$ excitons. Note that if lifetime effects are neglected, i.e., if all states but the three polariton branches are left aside, $\rho_\nu(\omega)$ is reduced to $\Sigma_\nu \delta(\omega - E_\nu)$, for $\nu =$ LP, MP, and UP, and the simple three-mode model for the RRS intensity is recovered.[19]

Using the Lehman representation of the Green's function[35] it can be shown that

$$\rho_{jl}(\omega) = -\frac{1}{2\pi}[G_{jl}(\omega + i0^+) - G_{jl}(\omega - i0^-)] = A_{\nu j}\bar{A}_{\nu l}\rho(\omega), \quad (13)$$

and taking into account that $\Sigma_j |A_{\nu j}|^2 = 1$, and that $\rho(\omega) = \Sigma_j \rho_{jj}(\omega)$, it can be followed by replacing these expressions in Eq. (12) that the desired equation for the Raman intensity is given by

$$I(\omega) \propto \frac{\rho_{ff}[\rho_{e1,e1} + |\alpha|^2 \rho_{e2,e2} + 2\,\mathrm{Re}(\alpha \rho_{e2,e1})]}{\sum_j \rho_{jj}}. \quad (14)$$

In the denominator we neglect the contribution of the continuum states, because it is negligible near the resonance condition for the outgoing polariton. Therefore the sum over j includes only the densities of excitons and photons. In particular if only two excitons are involved in the polariton system, we need to calculate only the diagonal Green's functions $G_{ff}(\omega)$, $G_{e1,e1}(\omega)$, $G_{e2,e2}(\omega)$, and also the crossed Green's function $G_{e2,e1}(\omega)$. Using the equations of motion we obtain

$$G_{ff}(\omega) = \frac{1}{\tilde{\omega}_f - \sum_i \dfrac{V_i^2}{\tilde{\omega}_i} - S_f'},$$

$$G_{e1,e1}(\omega) = \frac{1}{\tilde{\omega}_1 - \dfrac{V_1^2}{\tilde{\omega}_f - V_2^2/\tilde{\omega}_2}},$$

$$G_{e2,e2}(\omega) = \frac{1}{\tilde{\omega}_2 - \dfrac{V_2^2}{\tilde{\omega}_f - V_1^2/\tilde{\omega}_1}},$$

$$G_{e2,e1}(\omega) = G_{e1,e2}(\omega) = \frac{V_1 V_2}{\tilde{\omega}_1 \tilde{\omega}_2 \tilde{\omega}_f - V_1^2 \tilde{\omega}_2 - V_2^2 \tilde{\omega}_1}, \quad (15)$$

where

$$\tilde{\omega}_f = \omega - E_f - S_f, \quad \tilde{\omega}_i = \omega - E_{ei} - S_{ei}, \quad (16)$$

and

$$S_f(\omega) = \sum_p \frac{|V_p|^2}{\omega + i0^+ - \epsilon_p},$$

$$S_{ei}(\omega) = \sum_q \frac{|V_{iq}|^2}{\omega + i0^+ - \epsilon_{iq}},$$

$$S_f'(\omega) = \sum_k \frac{|V_k|^2}{\omega + i0^+ - \epsilon_k}. \quad (17)$$

For the first two of these sums, we assume that the results are imaginary constants that we take as parameters:

$$S_f(\omega) = -i\gamma_f, \quad S_j(\omega) = -i\gamma_{ej}. \quad (18)$$

This is the result expected for constant density of states and matrix elements. These two approximations are clearly not valid for the last sum. The last sum in Eq. (17) corresponds to the excitons that do not interact strongly with the MC photons, and to the electron-hole continuum. This continuum begins at the energy of the gap and corresponds to vertical transitions in which the light promotes a valence electron with 2D wave vector $k_\parallel$ to the conduction band with the same wave vector. In the effective-mass approximation, the energy ϵ_k is quadratic with $k_\parallel$ and this leads to a constant density of states beginning at the gap. As mentioned in the previous section, $V_k \sim \langle k_c | p_\sigma | k_v \rangle$. Approximating the wave functions as plane waves and averaging over all directions of $k_\parallel$ one has $\langle |V_k|^2 \rangle \sim k_\parallel^2 / 2$, proportional to the energy ϵ_k. Using these assumptions and separating $S_f'(\omega)$ in real $[r(\omega)]$ and imaginary $[y(\omega)]$ parts we can write

$$S_f'(\omega) = r(\omega) - iy(\omega), \quad r(\omega) = \frac{1}{\pi} \int d\epsilon \frac{y(\epsilon)}{(\omega - \epsilon)}, \quad (19)$$

$$y(\omega) = \mathcal{A}(\omega - E_{Xc})\Theta(\omega - E_{Xc}), \quad (20)$$

where E_{Xc} is the bottom of the electron-hole continuum, $\mathcal{A}$ is a dimensionless parameter that accounts for the coupling magnitude of the interaction between the MC photon and the continuum of excitations, and $\Theta(\omega)$ stands for the Heaviside function (step function). The real part $r(\omega)$ can be absorbed in a renormalization of the photon energy and is unimportant in what follows. The imaginary part $y(\omega)$ is a correction to the photon width for energies above the bottom of the continuum. From the formalism outlined above, this is expected to lead to a decrease in the RRS intensity when the energy is above the bottom of the continuum. The expression for $y(\omega)$ accounts so far only for effects of the exciton continuum, and leads therefore to a discontinuous first derivative of the calculated RRS profile. This discontinuity is overpassed, if the remaining bound exciton states are considered. To account for this infinite number of bound states, which become very dense below the bottom of the continuum, the lower part of $y(\omega)$ is replaced by a parabolic function that matches $(\omega - E_{Xc})$ with a continuous derivative, starting from zero at the energy (E_{X_c}'). At the energy E_{X_c}', which corresponds to the bottom of the electronic excitations in H_c, as described in the previous subsections,

$$y(\omega) = \begin{cases} 0 & \text{if } \omega \leq E'_{X_c} \\ \mathcal{A} \dfrac{(\omega - E'_{X_c})^2}{4(E_{Xc} - E'_{X_c})} & \text{if } E'_{X_c} \leq \omega \leq 2E_{Xc} - E'_{X_c} \\ \mathcal{A}(\omega - E_{Xc}) & \text{if } \omega \geq 2E_{Xc} - E'_{X_c}. \end{cases}$$

$$\tag{21}$$

As it will be shown in Sec. V, this refinement in the description of the continuum electron-hole electronic excitations and weakly bound excitons does not affect the Raman profile in resonance with the LP and MP branches, and only affects the resonant profile on the UP branch for energies above E'_{X_c}, leading to smoother curves.

The Raman intensity $I(\omega)$ for a fixed detuning is given by Eq. (14), together with Eqs. (13), (15)–(18), and (21), and its dependence with detuning (or equivalently with the spot position) enters through the corresponding variation of the bare MC photon (E_f) and exciton (E_{ei}) energies. In Sec. V we will discuss this model and compare the results to the above presented experimental data.

V. ANALYSIS AND DISCUSSION

The role of the cavity polaritons as intermediate states in the scattering process is fully displayed in the resonant enhancement of the Raman intensity as function of exciton-photon detuning, as described in Sec. III and shown in Fig. 2. Here the intensity of the scattered resonant Raman signal tuned to a polariton mode (the MP in this case) is followed continuously as this mode changes its character from very excitonic ($1s$-type) to photonic, and again very excitonic ($2s$-type).

In a simple picture, since the interaction of the polariton with the LO phonons is produced through the excitonic part of the polariton, the inelastic scattering process is favored when the polariton excitonic part is large. On the other hand the Stokes-shifted polariton is only detected when the polariton is transmitted outside of the sample. Since this coupling to the photon continuum is provided through the photonic part of the polariton, the Raman process is favored when this weight is also large. Thus in view of these two considerations, the process is optimized when a compromise between both situations is found, and this is reached at zero detuning, i.e., at the crossing of the bare exciton and MC photon, or what is equivalent at the energies where the differences $E_{MP} - E_{LP}$ or $E_{UP} - E_{MP}$ have a minimum. Thus, within this simplified picture, at these energies the RRS efficiency is maximized, and the scattered intensity decreases toward the pure excitonic and photonic limits. As we will see, the inclusion of photon and exciton lifetime broadening, i.e., the coupling of the MC photon to the exciton continuum described in Sec. IV, introduces important modifications to this correct but simplified view.

For comparison, the results of calculating the RRS intensity using the simple model given by Eq. (12) considering only three branches (with no lifetime broadening) are shown in Fig. 2(c) (dashed lines). Two maxima are displayed corresponding to the energy of the two anticrossings [compare to Fig. 2(b)]. This can be understood when the corresponding strength[38] components of the MP are analyzed [plotted in Fig. 1(b)]. The first anticrossing (~ 2.2 mm) happens at $E_f - E_{1s} = 0$ where $|A_f|^2 \simeq |A_{1s}|^2$ since the $2s$ strength at this position is very small. The second anticrossing (~ 3.4 mm) happens shortly before $E_f - E_{2s} = 0$, where the total exciton part equals the photonic part. As explained above at these points the compromise is found, and a maximal scattering intensity is expected within this model. As one can see in Fig. 2(c), this model qualitatively reproduces the general behavior well. However as pointed out before[18,19] many features are clearly *not* reproduced quantitatively. The first experimental maximum appears shifted (~ 2 meV) to higher energies, and something similar happens to the second peak, which appears shifted to lower energies (~ 1 meV) and less intense (shoulderlike), as indicated with arrows in Fig. 2(c). These observations can be assigned to lifetime or damping effects,[19] and point to the need of the polariton mediated Raman theory described in the previous section (Sec. IV B) that includes rigorously the lifetime broadening into the polariton states. In what follows, our experimental results will be compared to this theoretical model based on a Green's function approach.

The Raman intensity is given by Eq. (14), together with Eqs. (13) and (15)–(18). Parameters E_f, E_{1s}, and E_{2s} as function of the spot position x, as well as $2V_{1s} = \Omega_{f-1s}$ and $2V_{1s} = \Omega_{f-2s}$, were derived from the fit of the experimental dispersion shown in Fig. 1(a), using the result of the three-coupled-mode model as a seed. We estimated the bottom of the exciton continuum energy at $E_{Xc} \simeq 1.670$ meV. Parameter $\mathcal{A}$ is taken as 0.031, derived from the fit to Raman experiments in resonance with the UP on a similar II-VI cavity in the very strong coupling regime.[24] The line broadening of the noninteracting cavity photon is estimated by standard realistic reflectivity calculations[39,40] to be $\gamma_f \simeq 1$ meV. The exciton line broadening γ_{e1}, γ_{e2}, and the $2s - 1s$ ratio of the exciton-LO phonon interaction matrix elements given by α (assumed as a real number), together with the proportionality factor, are left as fitting parameters. Both types of experiments described in Sec. III [Fig. 2(c) and Fig. 4] are fitted *simultaneously*. Summarizing in a simple interpretation, the first experiment for varying spot position changes the photon-exciton character of the mediating polariton. While for the second experiment, the resonance scan at a fixed spot position (fixed detuning) accounts for the *total* polariton line broadening for that particular exciton-photon mixture. Best fits were obtained for $\gamma_{e1} = 1.2$ meV and $\gamma_{e2} = 0.9$ meV, and $\alpha = -0.45$. In Table I the parameters used for the calculations are summarized.

The resulting curves are shown for the RRS in Fig. 2(c) (full line) and for the resonant scans, respectively, in Fig. 4 (full lines). To fit the latter, only the upper half part of the scan has been used for the (b) and (c) scans, while for (a) the whole scan has been used. As can be observed the agreement with the measured data is very good, and provides a quantitative description. The obtained values for the parameters are relatively robust whether α, γ_{e1} or γ_{e2} are changed. For instance, a change of $\sim \pm 20\%$ on γ_{e1} leads to a shift of the RRS intensity maxima of ~ 0.5 meV toward higher or lower energies, respectively. Something similar occurs when γ_{e2} is changed, but the shift occurs in the opposite direction, i.e.,

TABLE I. Parameters used as input for the Raman resonant intensity calculations. The parameters indicated with an "*f*" in the last column were obtained from the fit to the data.

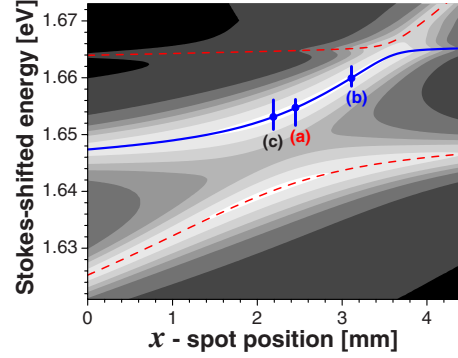| Parameter	Value
$\mathcal{A}$	0.031
γ_f	1 meV
γ_{e1}	1.2 meV *f*
γ_{e2}	0.9 meV *f*
α	-0.45 *f*

FIG. 5. (Color online) Contour plot of the total calculated outgoing Raman intensity. The LP and UP mode positions are indicated with dashed lines, and the MP outgoing resonant condition is plotted with a full curve. The Raman scans of Fig. 4 are indicated with vertical segments and labeled (a), (b), and (c), respectively. The intensity is given in logarithmic scale.

toward the direction where the polariton state has a stronger photonic character. The main influence on the RRS intensity profile of the parameter α is to regulate the relative intensity between the second and the first maxima. A change of $\pm20\%$ in this parameter increases or decreases the relative intensity in a 10%, respectively. An essential point in the fitting process is that since the 1*s*- and 2*s*-exciton weights for the three positions [scans (a), (c), and (b)] are different [see Fig. 1(b)], small changes in these parameters modify the width of the calculated Lorentzian-type curves obtained for a fixed detuning, changing consequently also the shape of the RRS scan. The simultaneous fit of both independent experiments determines unambiguously the way the values that these parameters can adopt.

A small discrepancy can be seen between the experimental and the theoretical intensities for very low detunings [see Fig. 2(c)], i.e., for low MP energies (<1.647 eV). The reasons for this discrepancy is attributed to the fact that for such low detuning the resonant MP polariton is extremely excitonic in its character, and this implies that its energy is almost that of a bare exciton. We presume that at this point the resonances with different excitonic states, which are not involved in the polaritonic state, start to contribute to the resonant Raman intensity. These excitonic resonances are not taken into account by our model, and it is therefore reasonable that the calculated curve [heavy line in Fig. 2(c)] falls below the experimental data.

A point that might seem odd at first sight is the fact that for the calculations γ_{e1} results slightly larger than γ_{e2}. Nevertheless, this result is to be expected if the origin of the broadening is disorder with a correlation length smaller or on the order of the 1*s* exciton's size:[31,32] The inhomogeneous broadening is substantially reduced by averaging over a volume larger than the length scale of the disorder potential. In fact, this is the reason why the disorder does not affect the broadening of the photons, the wavelength of which is much larger than the disorder correlation length.[32]

The total calculated Raman outgoing intensity is presented in Fig. 5 as a contour plot as function of the spot position (x) and the corresponding Stokes-shifted energy. The mode positions are indicated with dashed lines (LP and UP), and the MP outgoing resonant condition is plotted with a thick curve. In this figure the Raman intensity is shown in a logarithmic scale. The energies and x-positions of the Raman scans (shown in Fig. 4) are also indicated with vertical segments [marked as (a), (b), and (c), respectively], and the corresponding exact resonant position with a full circle. As

can be seen in this figure the Raman intensity decreases slightly asymmetrically when moving away from the exact MP Raman outgoing resonant condition when the Stokes-shifted energy is varied near the position of the first anticrossing, where the LP and MP modes are closer. It has to be pointed out that the calculated asymmetry points in the right direction, but is unfortunately not enough to account for the stronger one observed experimentally for Raman profiles (a) and (c). Something similar happens at the second anticrossing between the MP and UP, but in this case, due to the extremely low resonant outgoing Raman intensity on the UP, the anticrossing is not observable and is "washed out."

The same calculated total outgoing Raman intensity profile is presented in Fig. 6 as a three-dimensional plot. The mode positions (LP, MP) derived by projecting the corresponding resonance maxima on the xy plane are shown with dotted curves. For the case of the UP mode, as previously mentioned, it was not possible to determine the precise position of the RRS maximum of the UP at the second anticrossing. Thus, for this case, the curve shown corresponds to the one derived from the three-coupled-mode model [see Fig. 1(a)], which differs very little from the one derived by projecting the corresponding UP resonance maxima (where the UP resonance maxima are clearly distinguishable). The bottom panel of Fig. 6 shows a *rotated* detail of the UP region. The UP resonant profiles are presented highlighted. Here the upper Raman resonant peak is barely seen. For small x, the UP appears as a tiny peak that increases slightly its intensity when approximating the second anticrossing, and merging shoulderlike to the resonant profile coming from the MP, and increasing its energy after the anticrossing, decreasing its intensity. As can be derived from Fig. 1(a), for small x the UP has a strong excitonic character, which is conserved shortly before the second anticrossing. The photonic component of the UP at these energies is very small (see Fig. 6), and thus the coupling of the Stokes-shifted polaritons to the continuum of photonic states at the exterior of the cavity is very weak. When the position approaches the second anticrossing the photon-exciton mixture of the UP becomes larger, and therefore the Raman intensity increases, reaching
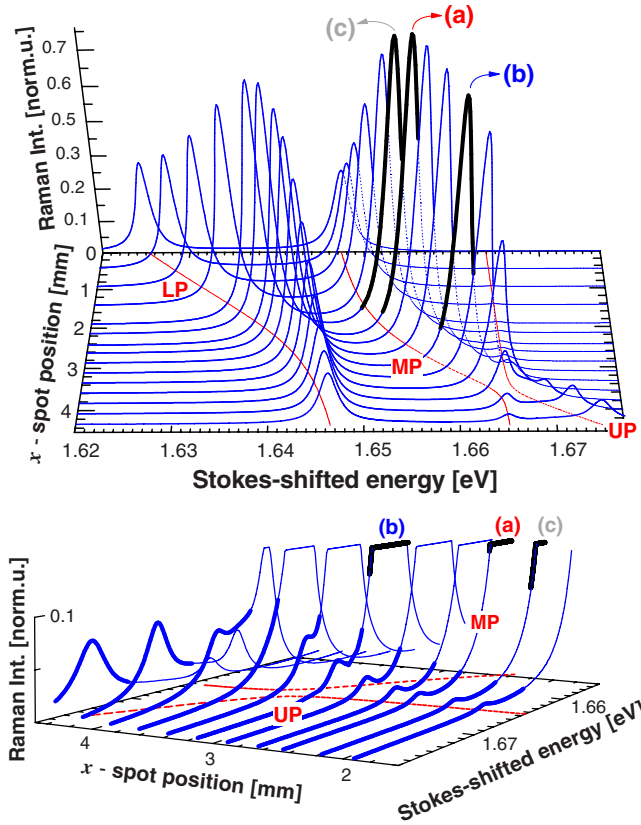
FIG. 6. (Color online) Three-dimensional plot of the calculated total outgoing Raman intensity profile as function of spot positions (x) and the corresponding Stokes-shifted energy. The full curves (LP, MP, and UP) projected on the xy plane of the plot indicate the polariton dispersion of the polariton branches. The highlighted resonance profiles on the MP marked as (a), (b), and (c) correspond, respectively, to the fitted curves in Fig. 4. The bottom panel shows a *rotated* detail of the UP region of the upper panel.

a broad maximum slightly after this anticrossing. For increasing energies, the coupling of the electron-hole continuum to this mode becomes larger and consequently its lifetime is reduced, the RRS intensity decreases, and the Raman profile becomes significantly broader.

As can be seen from Fig. 6, the scattered intensity for the outgoing resonant Raman condition with the UP is more than 1 order of magnitude smaller as compared to the situation in resonance with the MP. This extremely small light intensity scattered by the upper branch near the second anticrossing together with the important intensity loss due to the interaction of the polariton with the exciton continuum (as explained above) are the most probable reasons that hindered the experimental observation of this mode. For completeness, the fitted Raman intensity profiles of Fig. 4 are shown on the same plot, also highlighted by thicker lines and, respectively, indicated as (a), (b), and (c).

In our theory, we have not considered the possibility of polaritons of a higher branch to be scattered to lower polariton states. Since the LP is the lowest excited state of the system, the inclusion of this effect would cause an important increase in the LP resonant outgoing Raman intensity, with respect to the resonant scattered intensity by the higher order

polariton branches (MP, UP). This kind of effect has been reported by Tribe *et al.*[17] for a III-V type cavity with built-in electric field. The significantly larger contribution to the total scattered intensity coming from the LP may explain the asymmetry of the observed Raman scans and the discrepancies with the calculated curves (see Fig. 4), and would be particularly important at those situations where the LP and the MP are nearest, as is the case of the Raman scans labeled (a) and (c) in Figs. 4–6, i.e., near the first anticrossing.

A study of these processes, as well as detailed calculations of the different contributions to the exciton linewidth (supposed here as simple constants), and the careful determination of the exciton-LO phonon matrix elements (here accounted by the constant factor α), might lead to refinements and improvements of the theory. However, we believe that the formal framework of how the main physical ingredients enter the polariton mediated Raman process is well described by the above presented theory.

VI. CONCLUSIONS

Summarizing, we have reported two types of independent Raman experiments in near resonance with the middle cavity-polariton branch of a II-VI based semiconductor optical cavity. The first experiment shows the behavior of the Raman intensity at exact outgoing resonance with the cavity polariton, for varying photon-exciton detuning. In addition the second experiment shows the evolution for a fixed photon-exciton detuning, when the Stokes-shifted photons are tuned on and off resonance by varying the excitation energy. Both independent experiments are accounted *simultaneously* by the here developed cavity-polariton mediated Raman theory that rigorously includes photon and exciton damping effects. The presented theory describes quantitatively well the experimental results, a fact that remarks the importance of the exciton and cavity-photon lifetime effects in the process of inelastic scattering of light due to QW optical phonons. The shift of the Raman intensity maxima toward the situation where the polariton photonic strength is larger is one of the important features that are predicted by this model, and reasonable values for the damping constants are derived.

The theory in its present form is not able to explain the asymmetry of the observed Raman scans (see Fig. 4). It is possible that inelastic mechanisms of decay of the middle polariton in the lower one, not included here, might lead to an improvement of the comparison with experiment. Nevertheless, we believe that the presented Raman scattering theory based on a Green's function approach allows a consistent introduction of the damping mechanisms, and provides an important step forward in understanding this fundamental and interesting aspect of the inelastic light-matter interaction processes in optical microcavities.

*bruchhau@cab.cnea.gov.ar

†Also at CONICET, Argentina.

‡Present address: DPMC-MaNEP, Université de Genève, 24 Quai Ernest Ansermet, 1211 Genève 4, Switzerland.

[1] *Confined Electrons and Photon: New Physics and Applications*, edited by E. Burstein and C. Weisbuch (Plenum, New York, 1995).

[2] A. Kavokin and G. Malpuech, *Cavity Polaritons* (Elsevier, Amsterdam, 2003).

[3] Semicond. Sci. Technol. **18**, S279 (2003), special issue on microcavities, edited by J. J. Baumberg and L. Viña.

[4] See special issue, J. Phys.: Condens. Matter **16** (35), S3549 (2006).

[5] J. Kasprzak *et al.*, Nature (London) **443**, 409 (2006).

[6] R. Balili, V. Hartwell, D. Snoke, L. Pfeiffer, and K. West, Science **316**, 1007 (2007).

[7] H. Deng, D. Press, S. Götzinger, G. S. Solomon, R. Hey, K. H. Ploog, and Y. Yamamoto, Phys. Rev. Lett. **97**, 146402 (2006).

[8] A. Imamoglu and R. J. Ram, Phys. Lett. A **214**, 193 (1996).

[9] P. Senellart and J. Bloch, Phys. Rev. Lett. **82**, 1233 (1999).

[10] L. S. Dang, D. Heger, R. André, F. Boeuf, and R. Romestain, Phys. Rev. Lett. **81**, 3920 (1998).

[11] *Physics of Semiconductor Microcavities: From Fundamentals to Nanoscale Devices*, edited by B. Deveaud (Wiley, Berlin, 2006).

[12] M. M. de Lima, Jr., M. van der Poel, P. V. Santos, and J. M. Hvam, Phys. Rev. Lett. **97**, 045501 (2006).

[13] C. Weisbuch, M. Nishioka, A. Ishikawa, and Y. Arakawa, Phys. Rev. Lett. **69**, 3314 (1992).

[14] M. Cardona, in *Light Scattering in Solids II*, Topics in Applied Physics Vol. 50, edited by M. Cardona and G. Güntherodt (Springer-Verlag, Heidelberg, 1982).

[15] A. Fainstein, M. Trigo, D. Oliva, B. Jusserand, T. Freixanet, and V. Thierry-Mieg, Phys. Rev. Lett. **86**, 3411 (2001).

[16] A. Fainstein, B. Jusserand, and V. Thierry-Mieg, Phys. Rev. Lett. **78**, 1576 (1997).

[17] W. R. Tribe, D. Baxter, M. S. Skolnick, D. J. Mowbray, T. A. Fisher, and J. S. Roberts, Phys. Rev. B **56**, 12429 (1997).

[18] A. Fainstein, B. Jusserand, and R. André, Phys. Rev. B **57**, R9439 (1998).

[19] A. Bruchhausen, A. Fainstein, B. Jusserand, and R. André, Phys. Rev. B **68**, 205326 (2003).

[20] R. M. Stevenson, V. N. Astratov, M. S. Skolnick, J. S. Roberts, and G. Hill, Phys. Rev. B **67**, 081301(R) (2003).

[21] C. Weisbuch and R. G. Ulbrich, in *Light Scattering in Solids III*, Topics in Applied Physics Vol. 51, edited by M. Cardona and G. Güntherodt (Springer-Verlag, Heidelberg, 1998).

[22] A. Bruchhausen, A. Fainstein, and B. Jusserand, in *Physics of Semiconductors: 27th International Conference on the Physics of Semiconductors*, edited by J. Menéndez and C. G. Van de Walle, AIP Conf. Proc. No. 772 (AIP, New York, 2005), p. 1117.

[23] L. M. León Hilario, A. Bruchhausen, A. M. Lobos, and A. A. Aligia, J. Phys.: Condens. Matter **19**, 176210 (2007).

[24] L. M. León Hilario, A. A. Aligia, A. M. Lobos, and A. Bruchhausen, Superlattices Microstruct. **43**, 532 (2008).

[25] P. Y. Yu and M. Cardona, *Fundamentals of Semiconductors: Physics and Material Properies* (Springer-Verlag, Berlin, 1996).

[26] R. P. Stanley, R. Houdré, C. Weisbuch, U. Oesterle, and M. Ilegems, Phys. Rev. B **53**, 10995 (1996).

[27] This scan was shown in Ref. 19. The temperature was mistakenly indicated as 2.3 K, instead of 4.5 K.

[28] S. Jorda, U. Rössler, and D. Broido, Phys. Rev. B **48**, 1669 (1993).

[29] For this polarization the electric field couples to excitonic states with Γ_5 symmetry of the D_{2d} group (Ref. 28), corresponding in this case to the heavy-hole excitons states $1s$ and $2s$.

[30] A. Bruchhausen, A. Fainstein, B. Jusserand, and R. André, Phys. Rev. B **73**, 085305 (2006).

[31] D. M. Whittaker, P. Kinsler, T. A. Fisher, M. S. Skolnick, A. Armitage, A. M. Afshar, M. D. Sturge, J. S. Roberts, G. Hill, and M. A. Pate, Phys. Rev. Lett. **77**, 4792 (1996).

[32] D. M. Whittaker, Phys. Rev. Lett. **80**, 4791 (1998), and references therein.

[33] M. Shinada and S. Sugano, J. Phys. Soc. Jpn. **21**, 1936 (1966).

[34] Calvin Yi-Ping Chao and S. L. Chuang, Phys. Rev. B **43**, 6530 (1991).

[35] G. D. Mahan, *Many Particle Physics* (Kluver/Plenum, New York, 2000).

[36] K. Cho, in *Excitons*, Topics in Current Physics Vol. 14, edited by K. Cho (Springer-Verlag, Berlin, 1979).

[37] S. Jorda, Phys. Rev. B **50**, 2283 (1994).

[38] The strength is defined as the squared photonic or excitonic weight of the polariton, i.e. $|A_{\nu j}|^2$.

[39] P. Yeh, A. Yariv, and C.-S. Hong, J. Opt. Soc. Am. **67**, 423 (1976).

[40] A. Yariv, *Introduction to Optical Electronics* (Holt, Rinehart and Winston, New York, 1971).